

THIRD AND FOURTH STOKES PARAMETERS IN POLARIMETRIC PASSIVE MICROWAVE REMOTE SENSING OF ROUGH SURFACES OVER LAYERED MEDIA

Leung Tsang,¹ Peng Xu,^{2,3} and Kun Shan Chen²

¹ Department of Electrical Engineering, University of Washington, Seattle, WA 98195; Corresponding author: tsang@ee.washington.edu

² Center for Space and Remote Sensing Research, National Central University, Taiwan, Republic of China

³ School of Electronic Information, Wuhan University, Wuhan 430079, People's Republic of China

Received 19 April 2008

ABSTRACT: We consider the four Stokes parameters in microwave emission from a layered medium with the top interface being a rough surface. The rough surface varies in one horizontal direction so that azimuthal asymmetry exists in the 3-D problem. Dyadic Green's functions of multilayered media are used to formulate the surface integral equations. Periodic boundary conditions are used. The numerical results show that the presence of the layered media below the rough surface reduces the vertical and horizontal brightness temperatures. The interaction between the rough surface and the layered media also enhance the third and fourth Stokes parameters. In particular, the fourth Stokes parameter can be large for such geometrical configurations. Results show that the nonzero third and fourth Stokes parameters exist for all frequencies and are particularly large when the rough surface has large slope. © 2008 Wiley Periodicals, Inc. *Microwave Opt Technol Lett* 50: 3063–3069, 2008; Published online in Wiley InterScience (www.interscience.wiley.com). DOI 10.1002/mop.23892

Key words: polarimetric passive remote sensing; layered media; rough surface; emissivity

1. INTRODUCTION

WindSat, launched in January 2003, was the first spaceborne polarimetric radiometer to measure all four elements of Stokes vector, viz., the vertical polarized brightness temperatures, the horizontal polarized brightness temperatures, and the real and imaginary part of the cross-correlations of the vertical and horizontal polarizations [1]. It was shown by Tsang [2–4] that azimuthal asymmetry will create nonzero third and fourth Stokes parameters in passive microwave remote sensing. Thus the third and fourth Stokes parameters contain information of the azimuthal structure. This has the distinct advantage that such azimuthal structure is determined at a single azimuthal angle in polarimetric passive remote sensing. Usually the third and fourth Stokes parameters are quite small in airborne and spaceborne applications. In the past theoretical simulations of rough surface scattering, the third Stokes parameters can be large [5–7]. All these past work on rough surface emission have very small fourth Stokes parameter. On the other hand, the articles by Tsang [2–4] show that volume scattering by nonspherical scatterers can give large fourth Stokes parameter. Measurements of the Stokes parameters over Greenland show 10 K for the third Stokes parameter. They also show, for the first time, as large as between –10 and 20 K for the fourth Stokes parameter. The question is whether such large fourth Stokes parameter can be due to surface scattering and not volume scattering. In this article, we use numerical solution of Maxwell equations to study the problem of polarimetric passive microwave remote sensing of a random rough surface over multilayered structure. Our results show that interaction between rough surface scattering and reflection by layering can give large fourth Stokes parameter.

In Greenland, the wind induces azimuthal asymmetric rough surface known as the sastrugi. The sastrugi has rms height of 8–25 cm which is several microwave wavelengths from 10 to 37 GHz. Furthermore, the sastrugi has large slope. It is well known also that Greenland firm and Antarctica firm have multilayering structures that cause strong multiple reflections [8]. The multilayering structures have thicknesses of the order of several centimeters for each layer with each layer having a different density from the adjacent layers. Thus for the case of dry snow, microwaves can penetrate up to several meters at 10, 19, and 37 GHz. In the past, we have used a multilayered model to study such reflections and found significant decrease of emissivities due to these centimeters layering [8].

In Section 2, we use the surface integral equation approach to treat 3-D scattering, emission and absorption of a rough surface over multilayered media. The random rough surface is assumed to vary in only one horizontal direction so that azimuthal asymmetry exists in the 3-D problem. Dyadic Green's functions of multilayered medium [9] are used. The periodic boundary condition [10] is used instead of the usual tapered wave formulation. For the tapered wave, the wave is tapered horizontally over an extent of, say 3 m, at 10 GHz. However, surface reflections can occur as deep as 4–6 m, and such surface reflection can reach the surface outside the tapered wave extent. To account for the deep subsurface layering reflections, we use the periodic boundary condition which assumes an infinite surface. For the special case when the air-snow interface is smooth, the periodic boundary condition approach reduces to that of the layered medium while that of tapered wave does not. In Section 3, we give explicit expressions for the method of moment (MoM) discretizations of the matrix equation using pulse basis functions and point matching. In Section 4, numerical results are illustrated for polarimetric passive microwave remote sensing. The case of two layers and multilayers are illustrated. Results of all four Stokes parameters are shown for sinusoidal surface and sastrugi-type surface. For the case of large slopes of rough surface, it is shown that the interaction of rough surface with layering reflections can create large fourth Stokes parameter.

2. FORMULATIONS

Consider a periodic surface profile $z = f(x)$ over layered media as shown in Figure 1. Note that $d_1 > |\min f(x)|$ so that the first subsurface boundary will not intersect the rough surface. The region zero above the rough surface is air. The other layers are with permittivities of $\epsilon_1, \epsilon_2, \dots, \epsilon_N$, respectively. The incident

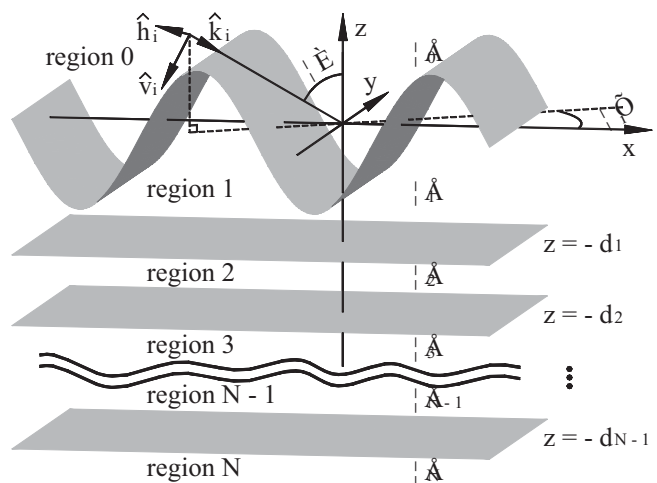


Figure 1 Geometry of a periodic surface over multilayered media

wave has a phase factor of $\exp(ik_{ix}x + ik_{iy}y - ik_{iz}z)$ making it a conical diffraction problem [10]. The incident electromagnetic fields are given by

$$\begin{cases} \bar{E}_i = E_{vi}\hat{v}_i + E_{in}\hat{h}_i \\ \eta\pi_i = E_{vi}\hat{h}_i - E_{in}\hat{v}_i \end{cases} \quad (1a)$$

$$(1b)$$

where

$$\begin{cases} E_{in} = \cos\alpha\exp(ik\bar{r}\cdot\hat{k}_i)\exp(-i\beta) \\ E_{vi} = \sin\alpha\exp(ik\bar{r}\cdot\hat{k}_i) \end{cases} \quad (2a)$$

$$(2b)$$

$$\begin{cases} \hat{k}_i = \sin\theta_i\cos\phi_i\hat{x} + \sin\theta_i\sin\phi_i\hat{y} - \cos\theta_i\hat{z} \\ \hat{h}_i = -\sin\phi_i\hat{x} + \cos\phi_i\hat{y} \\ \hat{v}_i = -\cos\theta_i\cos\phi_i\hat{x} - \cos\theta_i\sin\phi_i\hat{y} - \sin\theta_i\hat{z} \end{cases} \quad (3a)$$

$$(3b)$$

$$(3c)$$

The parameters α and β are used to characterize the polarizations. With the incident directions given above,

$$k_{ix} = k\sin\theta_i\cos\phi_i; k_{iy} = k\sin\theta_i\sin\phi_i; k_{iz} = k\cos\theta_i.$$

The integral equations are

$$\begin{aligned} \hat{y} \cdot \bar{E}_i(\bar{r}) + \iint_S dS' \hat{y} \cdot \nabla \times \bar{G}(\bar{r}, \bar{r}') \cdot \hat{n}' \times \bar{E}(\bar{r}') \\ + i\omega\mu\hat{y} \cdot \bar{G}(\bar{r}, \bar{r}') \cdot \hat{n}' \times \bar{H}(\bar{r}') = \begin{cases} \hat{y} \cdot \bar{E}(\bar{r}) & z > f(x) \\ 0 & z < f(x) \end{cases} \end{aligned} \quad (4a)$$

$$\begin{aligned} \iint_S dS' \hat{y} \cdot \nabla \times (\bar{G}_1(\bar{r}, \bar{r}') + \bar{G}_{1R}^{(m)}(\bar{r}, \bar{r}')) \cdot \hat{n}' \times \bar{E}_1(\bar{r}') \\ + i\omega\mu\hat{y} \cdot (\bar{G}_1(\bar{r}, \bar{r}') + \bar{G}_{1R}^{(e)}(\bar{r}, \bar{r}')) \cdot \hat{n}' \times \bar{H}_1(\bar{r}') \\ = \begin{cases} 0 & z > f(x) \\ -\hat{y} \cdot \bar{E}_1(\bar{r}) & z < f(x) \end{cases} \end{aligned} \quad (4b)$$

$$\begin{aligned} \hat{y} \cdot \bar{H}_i(\bar{r}) + \iint_S dS' \hat{y} \cdot \nabla \times \bar{G}(\bar{r}, \bar{r}') \cdot \hat{n}' \times \bar{H}(\bar{r}') \\ - i\omega\varepsilon\hat{y} \cdot \bar{G}(\bar{r}, \bar{r}') \cdot \hat{n}' \times \bar{E}(\bar{r}') = \begin{cases} \hat{y} \cdot \bar{H}(\bar{r}) & z > f(x) \\ 0 & z < f(x) \end{cases} \end{aligned} \quad (4c)$$

$$\begin{aligned} \iint \nabla \times (\bar{G}_1(\bar{r}, \bar{r}') + \bar{G}_{1R}^{(e)}(\bar{r}, \bar{r}')) \cdot \hat{n}' \times \bar{H}_1(\bar{r}') - i\omega\varepsilon_1\hat{y} \cdot (\bar{G}_1(\bar{r}, \bar{r}') \\ + \bar{G}_{1R}^{(m)}(\bar{r}, \bar{r}')) \cdot \hat{n}' \times \bar{E}_1(\bar{r}') = \begin{cases} 0 & z > f(x) \\ -\hat{y} \cdot \bar{H}_1(\bar{r}) & z < f(x) \end{cases} \end{aligned} \quad (4d)$$

where $\bar{G}(\bar{r}, \bar{r}')$ $\bar{G}_1(\bar{r}, \bar{r}')$ are 3-D dyadic Green's functions of homogeneous media, respectively, in region 0 and 1. $\bar{G}_{1R}^{(e)}$ $\bar{G}_{1R}^{(m)}$ $\times (\bar{r}, \bar{r}')$ are respectively electric and magnetic dyadic Green's function response in region 1 due to reflection of layered media below $z = -d_1$.

We have used the symmetry relations

$$(\bar{G}_{1R}^{(em)}(\bar{r}', \bar{r})) = \bar{G}_{1R}^{(em)}(\bar{r}, \bar{r}') \quad (5a)$$

$$(\nabla' \times \bar{G}_{1R}^{(em)}(\bar{r}', \bar{r})) = \nabla \times \bar{G}_{1R}^{(me)}(\bar{r}, \bar{r}') \quad (5b)$$

In (5a) and (5b), the superscript t denotes the transpose. The dyadic Green's functions are [9]

$$\begin{aligned} \bar{G}(\bar{r}, \bar{r}') = \frac{i}{8\pi^2} \iint dk_x dk_y \frac{1}{k_z} [\hat{e}(k_z)\hat{e}(k_z) + \hat{h}(k_z)\hat{h}(k_z)] \exp(ik_x(x \\ - x') + ik_y(y - y') + ik_z|z - z'|) \text{ for } z > z' \end{aligned} \quad (6a)$$

$$\begin{aligned} \bar{G}_1(\bar{r}, \bar{r}') = \frac{i}{8\pi^2} \iint dk_x dk_y \frac{1}{k_{1z}} \left[\begin{matrix} \hat{e}_1(-k_{1z})\hat{e}_1(-k_{1z}) + \\ \hat{h}_1(-k_{1z})\hat{h}_1(-k_{1z}) \end{matrix} \right] \exp(ik_x(x \\ - x') + ik_y(y - y') - ik_{1z}(z - z')) \text{ for } z < z' \end{aligned} \quad (6b)$$

$$\begin{aligned} \bar{G}_{1R}^{(e)}(\bar{r}, \bar{r}') = \frac{i}{8\pi^2} \iint dk_x dk_y \frac{1}{k_{1z}} \left[\begin{matrix} R^{TE}\hat{e}_1(k_{1z})\hat{e}_1(-k_{1z}) + \\ R^{TM}\hat{h}_1(k_{1z})\hat{h}_1(-k_{1z}) \end{matrix} \right] \exp(ik_x(x \\ - x') + ik_y(y - y') + ik_{1z}(z + z' + 2d_1)) \end{aligned} \quad (6c)$$

$$\begin{aligned} \bar{G}_{1R}^{(m)}(\bar{r}, \bar{r}') \\ = \frac{i}{8\pi^2} \iint dk_x dk_y \frac{1}{k_{1z}} \left[\begin{matrix} R^{TM}\hat{e}_1(k_{1z})\hat{e}_1(-k_{1z}) + \\ R^{TE}\hat{h}_1(k_{1z})\hat{h}_1(-k_{1z}) \end{matrix} \right] \exp(ik_x(x - x') \\ + ik_y(y - y') + ik_{1z}(z + z' + 2d_1)) \end{aligned} \quad (6d)$$

where

$$\hat{e}_1(\pm k_{1z}) = \frac{1}{k_p}(\hat{x}k_y - \hat{y}k_x) \quad (7a)$$

$$\hat{h}_1(\pm k_{1z}) = \pm \frac{k_{1z}}{k_1 k_p}(\hat{x}k_x + \hat{y}k_y) + \frac{k_p}{k_1}\hat{z} \quad (7b)$$

Reflection coefficients R^{TE} and R^{TM} of region 1 are due to response from the multilayers regions below $z = -d_1$.

Because of uniformity in the \hat{y} direction, the $\exp(ik_{iy}y)$ dependence is common and can be cancelled out from Eqs. (4a)–(4d). Let the surface unknowns be the \hat{y} components of surface electric and magnetic fields and their normal derivatives in region 1.

$$\begin{cases} \varphi_1(x) = H_{1yw}(x, z = f(x)) \end{cases} \quad (8a)$$

$$\begin{cases} \xi_1(x) = [\hat{n}_j \cdot \nabla_j H_{1yw}(x, z)]_{z=f(x)} \end{cases} \quad (8b)$$

$$\begin{cases} \psi_1(x) = E_{1yw}(x, z = f(x)) \end{cases} \quad (8c)$$

$$\begin{cases} \chi_1(x) = [\hat{n}_i \cdot \nabla_i E_{1yw}(x, z)]_{z=f(x)} \end{cases} \quad (8d)$$

where $H_{1yw}\exp(ik_{iy}y) = H_{1y}$ $E_{1yw}\exp(ik_{iy}y) = E_{1y}$

The surface unknowns from region 0, $\varphi(x)$, $\xi(x)$, $\psi(x)$, $\chi(x)$, have similar definitions.

The boundary conditions are that

$$\psi(x) = \psi_1(x) \quad (9a)$$

$$\varphi(x) = \varphi_1(x) \quad (9b)$$

$$\chi(x) = \frac{c_0}{\sqrt{1 + (f'(x))^2}} \frac{d(\eta\varphi_1(x))}{dx} + c_2\chi_1(x) \quad (9c)$$

$$\eta\xi(x) = -\frac{d_0}{\sqrt{1 + (f'(x))^2}} \frac{d\psi_1(x)}{dx} + d_2\eta\xi_1(x) \quad (9d)$$

where η is wave impedance in free space, and

$$c_0 = d_0 - \frac{k_n}{k} \left(\frac{k_r^2}{k_{1r}^2} - 1 \right) \quad (10a)$$

$$c_2 = \frac{\varepsilon_1 k_1^2}{\varepsilon k_{1r}^2} \quad (10b)$$

$$d_2 = \frac{k_i^2}{k_{1r}^2} \quad (10c)$$

$$k_{j_i} = \sqrt{k_j^2 - k_{iy}^2} \quad j = 0, 1 \quad (10d)$$

After considerable simplifications, we obtain the following surface integral equations

$$\frac{1}{2} \psi(x) - \int_L ds' g_p(x') \hat{n}'_i \cdot \nabla'_i g_p + \int \int ds' g_p \chi(x') = E_{iyw}(x, z) \quad (11a)$$

$$\begin{aligned} & \int_L ds' [\bar{Q}_{1R}^{(m)}(x, z; x' z') \cdot \hat{n}' \times \bar{E}_{1w}(x') + i\omega\mu \bar{P}_{1R}^{(e)}(x, z, x, z') \cdot \hat{n}' \\ & \times \bar{H}_{1w}(x')] + \int_L ds' \psi p(x') \hat{n}' \cdot \nabla' \text{tg} 1P \\ & - \int_L ds' g_{1p} \chi_1(x') = 0 \end{aligned} \quad (11b)$$

$$\frac{1}{2} \varphi(x) - \int_L ds' \varphi(x') \hat{n}'_i \cdot \nabla'_i g_p + \int_L ds' g_p \xi(x') = H_{iyw}(x, z) \quad (11c)$$

$$\begin{aligned} & \int_L ds' [\bar{Q}_{1R}^{(e)}(x, z; x' z') \cdot \hat{n}' \times \bar{H}_{1w}(x') - i\omega\varepsilon_1 \bar{P}_{1R}^{(m)}(x, z; x' z') \cdot \hat{n}' \\ & \times \bar{E}_{1w}(x')] + \frac{1}{2} \varphi_1(x) + \int_L ds' \varphi_1(x') \hat{n}'_i \cdot \nabla'_i g_{1p} - \int_L ds' g_{1p} \xi_1(x') \\ & = 0 \end{aligned} \quad (11d)$$

where \int denotes a principle value of integral. g_p and g_{1p} are 2-D periodic Green's functions, respectively, in region 0 and 1,

$$g_{jp}(x, z; x' z') = \frac{i}{2L} \sum_{m=-\infty}^{\infty} \frac{\exp(ik_{xm}(x-x') + ik_{jzm}|z-z'|)}{k_{jzm}} \quad (12)$$

for $j = 0, 1$.

The Floquet mode is governed by the relations

$$k_{xm} = k_{ix} + m \frac{2\pi}{L} \quad (13a)$$

$$k_{jzm} = \sqrt{k_i^2 - k_{iy}^2 - k_{xjm}^2} = 0, 1 \quad (13b)$$

where L is the length of the period in the periodic boundary condition.

In the above equation, using Poisson's Summation,

$$\begin{aligned} \bar{P}_{1R}^{(e)}(x, z; x' z') &= \sum_n \exp(ik_{ix} nL - ik_{iy} y) \int_{-\infty}^{\infty} dy' \hat{y} \cdot \bar{G}_{1R}^{(e)} \\ &\times (\bar{r}, \bar{r}') \exp(ik_{iy} y') = \\ &- \frac{i}{2L} \sum_{m=-\infty}^{\infty} \frac{\exp(ik_{xm}(x-x') + ik_{1zm}(z+z'+2d_1))}{k_{\rho m}^2} \\ &\times \left[R_{k_m}^{11} \frac{k_{xm}}{k_{1zm}} (\hat{x}k_n - \hat{y}k_{xm}) + R_{k_{\rho m}}^{TM} \frac{k_{iy} k_{1zm}}{k_1^2} (\hat{x}k_{xm} + \hat{y}k_n + \hat{z} \frac{k_{\rho m}^2}{k_{1zm}}) \right] \end{aligned} \quad (14a)$$

$$\begin{aligned} \bar{Q}_{1R}^{(e)}(x, z; x' z') &= \sum_n \exp(ik_{ix} nL - ik_{iy} y) \int_{-\infty}^{\infty} dy' \hat{y} \cdot \nabla \times \bar{G}_{1R}^{(e)} \\ &\times (\bar{r}, \bar{r}') \exp(ik_{iy} y') = \\ &- \frac{1}{2L} \sum_{m=-\infty}^{\infty} \frac{\exp(ik_{xm}(x-x') + ik_{1zm}(z+z'+2d_1))}{k_{\rho m}^2} \\ &\times \left[R_{k_{\rho m}}^{TM} k_{xm} (\hat{x}k_n - \hat{y}k_{xm}) - R_{k_{\rho m}}^{TM} k_{xm} (\hat{x}k_{xm} + \hat{y}k_{iy} + \hat{z} \frac{k_{\rho m}^2}{k_{1zm}}) \right] \end{aligned} \quad (14b)$$

where

$$k_{\rho m} = \sqrt{k_{xm}^2 + k_{iy}^2} \quad (15)$$

$R_{k_{\rho m}}^{TE}$ and $R_{k_{\rho m}}^{TM}$ are the TE and TM reflection coefficients, respectively, and are evaluated at the Floquet mode of $k_{\rho m}$. $\bar{P}_{1R}^{(m)}$ and $\bar{Q}_{1R}^{(m)}$ have expressions similar to $\bar{P}_{1R}^{(e)}$ and $\bar{Q}_{1R}^{(e)}$ except for the interchange of $R_{k_{\rho m}}^{TE}$ and $R_{k_{\rho m}}^{TM}$.

3. MATRIX EQUATIONS IN METHOD OF MOMENT

Next, we apply the MoM with pulse basis functions and point matching at the center point x_n of each pulse basis function. Because the rough surface can have large slope, we discretize the surface such that each segment has equal surface length of $\Delta l = \Delta x_n \sqrt{1 + (f'(X_n))^2}$ so that the points are not equally spaced on the x axis. Let N be the number of points of discretization, then we obtain the following matrix equation of dimensions $4N \times 4N$.

$$\begin{bmatrix} \bar{A} & c_2 \bar{B} & -c_0 \bar{C} & \bar{0} \\ \bar{D} + \bar{I} & \bar{E} + \bar{H} & \bar{F} & \bar{J} \\ d_0 \bar{C} & \bar{0} & \bar{A} & d_2 \bar{B} \\ \bar{Y} & \bar{U} & \bar{D} + \bar{W} & \bar{E} + \bar{Z} \end{bmatrix} \begin{bmatrix} \bar{\psi}_1 \\ \bar{\chi}_1 \\ \eta \bar{\varphi}_1 \\ \eta \bar{\xi}_1 \end{bmatrix} = \begin{bmatrix} \bar{E}_{iyw} \\ \bar{0} \\ \eta \bar{H}_{iyw} \\ \bar{0} \end{bmatrix} \quad (16)$$

where

$$A_{mn} = \begin{cases} \frac{1}{2} - \Delta x_n \left[f'(x_n) \frac{\partial g'_p}{\partial X} - \frac{\partial g'_p}{\partial Z} \right]_{x=0, Z=0} & \text{for } m = n \\ \Delta x_n \left[f'(x_n) \frac{\partial g_p}{\partial X} - \frac{\partial g_p}{\partial Z} \right] & \text{for } m \neq n \end{cases} \quad (17)$$

$$B_{mn} = \begin{cases} \Delta \ell \left[\frac{i}{4} \left(1 + 2 \frac{i}{\pi} \log \frac{\gamma k_i \Delta \ell}{4e} \right) + g'_p \left(\begin{matrix} X=0 \\ Z=0 \end{matrix} \right) \right] & \text{for } m = n \\ \Delta \ell g_p(x_m f(x_m); x_n f(x_n)) & \text{for } m \neq n \end{cases} \quad (18)$$

$$C_{mn} = g_p \left(x_m f(x_m); x_n + \frac{\Delta x_n}{2} f \left(x_n + \frac{\Delta x_n}{2} \right) \right) \quad Z_{mn} = -\Delta \ell \frac{k_1^2}{k_{1t}^2} \bar{P}_{1R}^{(m)}(X, Z) \cdot \hat{y} \quad (29)$$

$$- g_p \left(x_m f(x_m); x_n - \frac{\Delta x_n}{2} f \left(x_n - \frac{\Delta x_n}{2} \right) \right) \quad (19) \quad \hat{n}_n = \frac{-f'(x_n)\hat{x} + \hat{z}}{\sqrt{1 + (f'(x_n))^2}} \quad (30)$$

$$D_{mn} = \begin{cases} \frac{1}{2} + \Delta x_n \left[f'(x_n) \frac{\partial g'_{1p}}{\partial X} - \frac{\partial g'_{1p}}{\partial Z} \right]_{X=0, Z=0} & \text{for } m = n \\ \Delta x_n \left[f'(x_n) \frac{\partial g_{1p}}{\partial X} - \frac{\partial g_{1p}}{\partial Z} \right] & \text{for } m \neq n \end{cases} \quad g'_p(X, Z) = g_p(X, Z) - \frac{i}{4} H_0^{(1)}(k_t \sqrt{X^2 + Z^2}) \quad (31a)$$

$$g'_{1p}(X, Z) = g_{1p}(X, Z) - \frac{i}{4} H_0^{(1)}(k_{1t} \sqrt{X^2 + Z^2}) \quad (31b)$$

$$E_{mn} \quad X = x_m - x_n \quad (32a)$$

$$= \begin{cases} -\Delta \ell \left[\frac{i}{4} \left(1 + 2 \frac{i}{\pi} \log \frac{\gamma k_{1t} \Delta \ell}{4e} \right) + g_{1p}' \left(\frac{X=0}{Z=0} \right) \right] & \text{for } m = n \\ -\Delta \ell g_{1p}(x_m, f(x_m), x_n, f(x_n)) & \text{for } m \neq n \end{cases} \quad Z = \begin{cases} f(x_m) - f(x_n) & \text{for } \bar{A}, \bar{B}, \bar{C}, \bar{D}, \bar{E} \\ f(x_m) + f(x_n) & \text{for } \bar{F}, \bar{J}, \bar{H}, \bar{I}, \bar{U}, \bar{Y}, \bar{W}, \bar{Z} \end{cases} \quad (32b)$$

Note that g'_p and g'_{1p} are the periodic Green's function minus the contribution from the zeroth period so that they are not singular at argument equal to zero. The change to $f(x_m) + f(x_n)$ in $\bar{F}, \bar{J}, \bar{H}, \bar{I}, \bar{U}, \bar{Y}, \bar{W}$, and \bar{Z} are because these matrix elements represent subsurface reflections.

$$F_{mn} = ik \Delta \ell (\bar{P}_{1R}^{(e)}(X, Z)) \cdot \hat{n}_n \times \hat{y} + \frac{kk_{iy}}{k_{1t}^2} \left[\bar{P}_{1R}^{(e)} \left(x_m f(x_m), x_n + \frac{\Delta x_n}{2} f \left(x_n + \frac{\Delta x_n}{2} \right) \right) - \bar{P}_{1R}^{(e)} \left(x_m f(x_m), x_n - \frac{\Delta x_n}{2} f \left(x_n - \frac{\Delta x_n}{2} \right) \right) \right] \cdot \hat{y} \quad (22)$$

We used the method of Veysoglu et al. [5, 10] for fast computation of the homogeneous periodic Green's function g_p and g_{1p} . For the layered media periodic Green's function of the reflective part, $\bar{P}_{1R}^{(e)}$, $\bar{Q}_{1R}^{(e)}$, $\bar{P}_{1R}^{(m)}$ and $\bar{Q}_{1R}^{(m)}$, they are computed by using the spectral domain representations which converge rapidly.

$$J_{mn} = -\Delta \ell \frac{ik}{k_{1t}^2} \bar{Q}_{1R}^{(m)}(X, Z) \cdot \hat{y} \quad (23)$$

After the surface fields are determined, the coefficients of reflected Floquet modes can be calculated. For the m th Floquet mode of the scattered wave,

$$I_{mn} = \Delta \ell (\bar{Q}_{1R}^{(m)}(X, Z)) \cdot \hat{n}_n \times \hat{y} - \frac{k_{iy}}{k_{1t}^2} \left[\bar{Q}_{1R}^{(m)} \left(x_m f(x_m), x_n + \frac{\Delta x_n}{2} f \left(x_n + \frac{\Delta x_n}{2} \right) \right) - \bar{Q}_{1R}^{(m)} \left(x_m f(x_m), x_n - \frac{\Delta x_n}{2} f \left(x_n - \frac{\Delta x_n}{2} \right) \right) \right] \cdot \hat{y} \quad (24)$$

$$E_{xsm} = -\frac{1}{2L} \sum_n \exp(-ik_{xm}x_n - ik_{zm}f(x_n)) \left[\frac{ic_2}{k_{zm}} \chi_{1n} \Delta \ell - c_0 \eta \varphi_{1n} \left(\frac{k_{xm}}{k_{zm}} + f'(x_n) \right) \Delta x_n + \psi_{1n} \left(\frac{k_{xm}}{k_{zm}} f'(x_n) - 1 \right) \Delta x_n \right] \quad (33a)$$

$$H_{mn} = -\Delta \ell \frac{k_1^2}{k_{1t}^2} \bar{P}_{1R}^{(e)}(X, Z) \cdot \hat{y} \quad (25)$$

$$\eta H_{ysm} = -\frac{1}{2L} \sum_n \exp(-ik_{xm}x_n - ik_{zm}f(x_n)) \left[\frac{id_2}{k_{zm}} \eta \xi_{1n} \Delta \ell + d_0 \psi_{1n} \left(\frac{k_{xm}}{k_{zm}} + f'(x_n) \right) \Delta x_n + \eta \varphi_{1n} \left(\frac{k_{xm}}{k_{zm}} f'(x_n) - 1 \right) \Delta x_n \right] \quad (33b)$$

$$U_{mn} = \Delta \ell \frac{i \varepsilon_1 k}{\varepsilon k_{1t}^2} \bar{Q}_{1R}^{(e)}(X, Z) \cdot \hat{y} \quad (26)$$

Given the polarization α , E_{vi} , E_{hi} of the incident wave, the reflectivity is

$$Y_{mn} = -ik \frac{\varepsilon_1}{\varepsilon} \Delta 517 (\bar{P}_{1R}^{(m)}(X, Z)) \cdot \hat{n}_n \times \hat{y} - \frac{\varepsilon_1 k k_{iy}}{\varepsilon k_{1t}^2} \left[\bar{P}_{1R}^{(m)} \left(x_m f(x_m), x_n + \frac{\Delta x_n}{2} f \left(x_n + \frac{\Delta x_n}{2} \right) \right) - \bar{P}_{1R}^{(m)} \left(x_m f(x_m), x_n - \frac{\Delta x_n}{2} f \left(x_n - \frac{\Delta x_n}{2} \right) \right) \right] \cdot \hat{y} \quad (27)$$

$$r_\alpha(\theta_i, \varphi_i) = \frac{k}{k_t^2} \frac{\sum_m k_{zm} (|\eta H_{ysm}|^2 + |E_{ysm}|^2)}{(|E_{vi}|^2 + |E_{hi}|^2) \cos \theta_i} \quad (34)$$

where the summation in (34) over the Floquet modes is only over the propagating waves and not the evanescent waves.

The emissivity of the α polarization is

$$e_\alpha(\theta_i, \varphi_i) = 1 - r_\alpha(\theta_i, \varphi_i) \quad (35)$$

The absorptivity is

$$W_{mn} = \Delta \ell (\bar{Q}_{1R}^{(e)}(X, Z)) \cdot \hat{n}_n \times \hat{y} - \frac{k_{iy}}{k_{1t}^2} \left[\bar{Q}_{1R}^{(e)} \left(x_m f(x_m), x_n + \frac{\Delta x_n}{2} f \left(x_n + \frac{\Delta x_n}{2} \right) \right) - \bar{Q}_{1R}^{(e)} \left(x_m f(x_m), x_n - \frac{\Delta x_n}{2} f \left(x_n - \frac{\Delta x_n}{2} \right) \right) \right] \cdot \hat{y} \quad (28)$$

$$a_\alpha(\theta_i, \varphi_i) = \frac{k \Delta \ell \text{Im} \sum_n [\psi(x_n) \chi^*(x_n) - \eta^2 \varphi^*(x_n) \xi(x_n)]}{k_t^2 L \cos \theta_i (|E_{vi}|^2 + |E_{hi}|^2)} \quad (36)$$

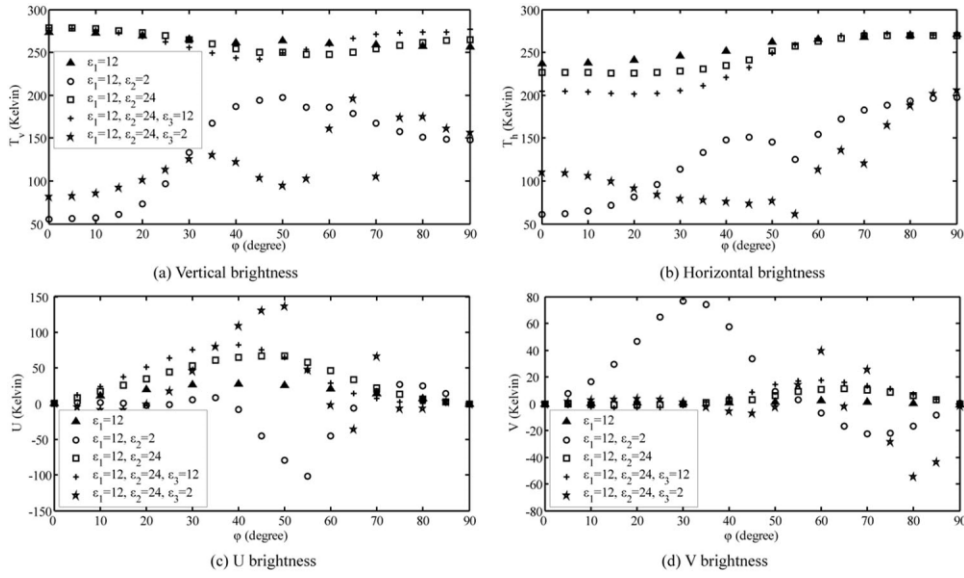


Figure 2 Brightness temperatures at polar angle $\theta_i = 20^\circ$ at frequency of 1 GHz with physics temperature $T_0 = 300$ K versus azimuthal angle. Rough surface is with $z = 15 \sin(2\pi x/50)$ cm. \blacktriangle : rough surface alone; \circ : over a single layer with $d_1 = 16.8$ cm and small ϵ_2 ; \square : over a single layer with $d_1 = 16.8$ cm and large ϵ_2 ; $+$: over two layers with $d_1 = 16.8$ cm, $d_2 = 26.8$ cm and large ϵ_3 ; $*$: over two layers with $d_1 = 16.8$ cm, $d_2 = 26.8$ cm and small ϵ_3

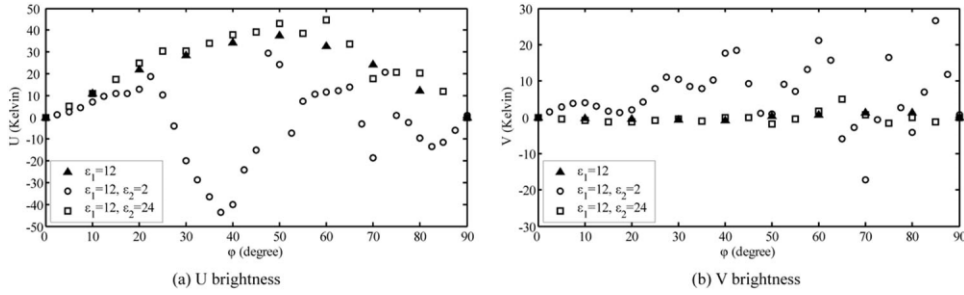


Figure 3 Brightness temperatures versus azimuthal angle. $\theta_i = 20^\circ$, freq = 5 GHz, $T_0 = 300$ K. Rough surface is with $z = 15 \sin(2\pi x/50)$ cm. \blacktriangle : rough surface alone; \circ : over a single layer with $d_1 = 16.8$ cm and small ϵ_2 ; \square : over a single layer with $d_1 = 16.8$ cm and large ϵ_2

using the surface unknowns from region 0. Energy conservation check is performed by verifying that $r_\alpha(\theta_i, \varphi_i) + a_\alpha(\theta_i, \varphi_i) = 1$.

For polarizations, let $\alpha = v, h, +45^\circ, -45^\circ, RC, LC$ be polarizations of vertical, horizontal, $+45^\circ$ linear, -45° linear, right-hand circular, and left-hand circular polarization, respectively. The brightness temperatures are related to the emissivities by

$$T_\alpha(\theta_i, \varphi_i) = e_\alpha(\theta_i, \varphi_i) T_0 \quad (37)$$

where T_0 is the physical temperature. The four Stokes parameters are $T_h, T_v, U = T_{45} - T_{-45}$, and $V = T_{LC} - T_{RC}$.

4. NUMERICAL RESULTS AND DISCUSSION

We first follow reference [5], and use a sinusoidal profile $f(x) = A \sin(2\pi x/L)$, with $A = 0.15$ m and $L = 0.5$ m. In Figures 2 and 3, we show the dependence on azimuthal angle of all four Stokes parameters, respectively, at 1 and 5 GHz for several layering structures. The incident observation angle θ_i is 20° and physical temperature is at 300 K. For comparison, the results for the half space (without layering) with rough surface are also shown.

Results in Figure 2 show that because of reflections with layering, the vertical, and horizontal brightness temperatures are less than those without layering. When permittivity in region 2 is less than that in region 1, not only its third Stokes parameter U can

be as large as -102 K, but also that the fourth Stokes parameter V can be up to 77 K. If ϵ_2 is larger than ϵ_1 , U and V both decrease, particularly for V , though they are still larger than those without layers. Results show that the fourth Stokes parameter can be large if there is a layer with permittivity smaller than that of medium 1. This indicates that the fourth Stokes parameter can be created by total internal reflections. Figure 3 shows the third and fourth Stokes parameters at 5 GHz. They are still large. This means that the nonzero third and fourth Stokes parameter exist for all fre-

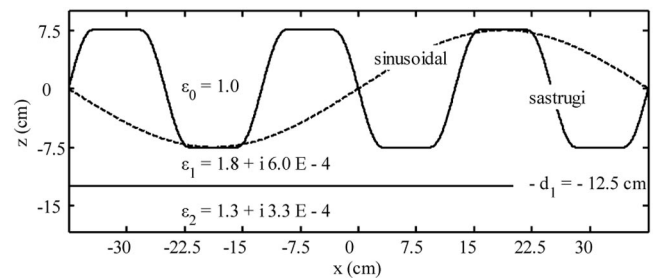


Figure 4 Sastrugi profile (solid line, height = 15 cm, period = 25 cm, large slope) and sinusoidal profile (dash line, height = 15 cm, period = 75 cm, small slope) over a single layer with $-d_1 = -12.5$ cm

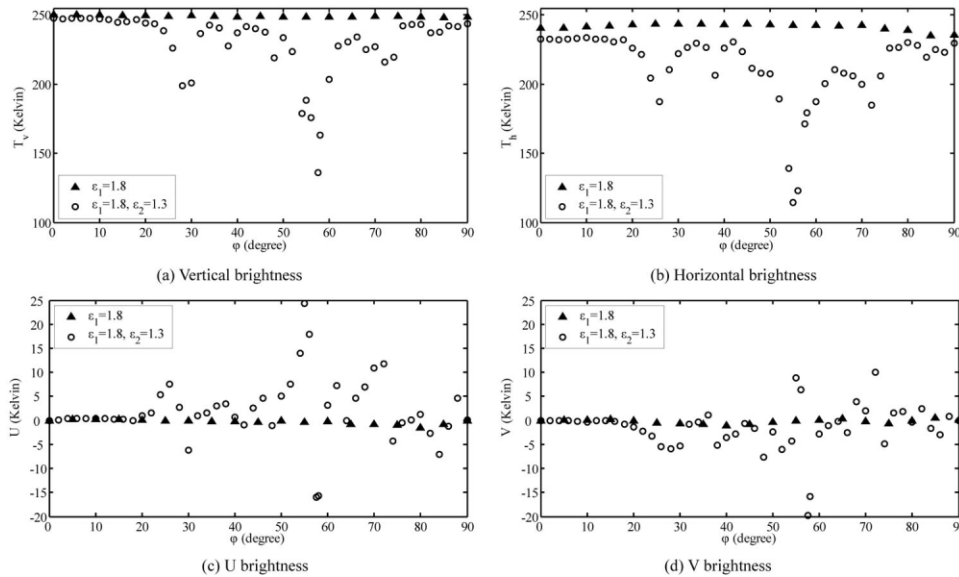


Figure 5 Brightness temperatures versus azimuthal angle. $\theta_i = 55^\circ$, $\text{freq} = 10 \text{ GHz}$, $T_0 = 250 \text{ K}$. Sastrugi rough surface is shown in Figure 4. Height = 15 cm, period = 25 cm \blacktriangle : rough surface alone; \circ : over a single layer

quencies because total internal reflection is an effect of geometric optics.

A sastrugi-type surface is depicted in Figure 4. The sastrugi surface in a period L has

$$f(x) = \begin{cases} A \sin(4\pi x/L) & \text{for } -5L/8 < x \leq -3L/8 \\ A & \text{for } -3L/8 \leq x \leq -L/8 \\ -A \sin(4\pi x/L) & \text{for } -L/8 \leq x \leq L/8 \\ -A & \text{for } L/8 \leq x < 3L/8 \end{cases} \quad (38)$$

The surface height is $2A = 15 \text{ cm}$, and the period is $L = 25 \text{ cm}$. We consider the case at 10 GHz, at the incident angle $\theta_i = 55^\circ$. The physical temperature is set at 250 K. The permittivities are set as snow with a small imaginary part. As shown in Figure 5, for the case without layering, the vertical and horizontal polar brightness vary little with azimuthal angle, and the third and fourth brightness are very small. However, if a layer with smaller permittivity $\epsilon_2 = 1.3 + i3.3E-4$ is put below at $-d_1 = -12.5 \text{ cm}$, then U can be as large as 24.4 K and V can be as large as -19.8 K . The vertical and horizontal brightness temperatures can decrease.

In Figure 6, we show that the third and fourth Stokes param-

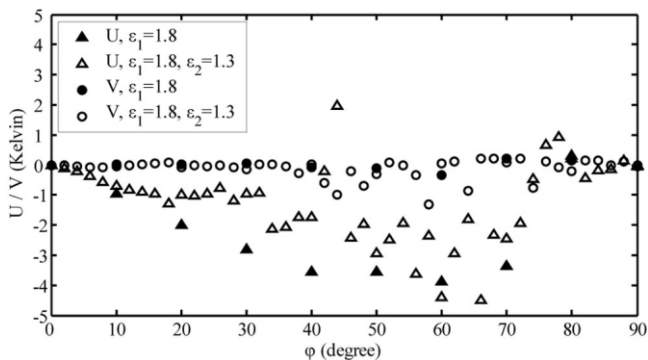


Figure 6 Brightness temperatures versus azimuthal angle. $\theta_i = 55^\circ$, $\text{freq} = 10 \text{ GHz}$, $T_0 = 250 \text{ K}$. Sinusoidal rough surface is shown in Figure 4 too. Height = 15 cm, period = 75 cm \blacktriangle , \bullet : rough surface alone; \triangle , \circ : over a single layer

eters with the same parameters as those of Figure 5 except that the sastrugi surface is replaced by a sinusoidal profile with small slope that has $2A = 15 \text{ cm}$ and period $L = 75 \text{ cm}$. The sinusoidal profile is also shown in Figure 4. Because of the small difference of snow permittivities between layers, the reflection from the layer boundaries cannot cause large third and fourth Stokes parameters without the large slopes in the rough surface.

ACKNOWLEDGMENTS

The research in this paper was supported by the US National Science Foundation.

REFERENCES

1. P.W. Gaiser, K.M. St Germain, E.M. Twarog, G.A. Poe, W. Purdy, D. Richardson, W. Grossman, W.L. Jones, D. Spencer, G. Golba, J. Cleveland, L. Choy, R.M. Bevilacqua, and P.S. Chang, The WindSat spaceborne polarimetric microwave radiometer: sensor description and early orbit performance, *IEEE Trans Geosci Remote Sens* 42 (2004), 2347–2361.
2. L. Tsang, Thermal emission of nonspherical particles, *Radio Sci* 19, (1984), 966–974.
3. L. Tsang and Z. Chen, Polarimetric passive and active remote sensing: Theoretical modeling of random discrete scatterers and rough surfaces, *Proceedings of IEEE International Geoscience and Remote Sensing Symposium (IGARSS'90)*, pp. 2201–2203, May 1990.
4. L. Tsang, Polarimetric passive microwave remote sensing of random discrete scatterers and rough surfaces, *J Electromagn Waves Appl* 5 (1991), 41–57.
5. M.E. Veysoglu, H.A. Yueh, R.T. Shin, and J.A. Kong, Polarimetric passive remote sensing of periodic surfaces, *J Electromagn Waves Appl* 5 (1991), 267–280.
6. L. Li, C.H. Chan, and L. Tsang, Numerical simulation of conical diffraction of tapered electromagnetic waves from random rough surfaces and applications to passive remote sensing, *Radio Sci* 29 (1994), 587–598.
7. J.T. Johnson, J.A. Kong, R.T. Shin, D.H. Staelin, K. O'Neill, and A.W. Lohanick, Third Stokes parameter emission from a periodic water surface, *IEEE Trans Geosci Remote Sens* 31 (1993), 1066–1080.

8. R.D. West, D.P. Winebrenner, L. Tsang, and H. Rott, Microwave emission from density stratified Antarctic firn at 6 cm wavelength, *J Glaciol* 42 (1996), 63–76.
9. L. Tsang, J.A. Kong, and K.H. Ding, *Scattering of electromagnetic waves, Vol. 1: Theory and applications*, Wiley Interscience, New York, NY, 2000.
10. L. Tsang, J.A. Kong, K.H. Ding and C.O. Ao, *Scattering of electromagnetic waves, Vol. 2: Numerical simulations*, Wiley Interscience, New York, NY, 2001.

© 2008 Wiley Periodicals, Inc.

ANALYSIS OF V-SLOT LOADED PATCH FOR WIDE-BAND OPERATION

J. A. Ansari,¹ Satya Kesh Dubey,¹ Prabhakar Singh,¹
R. U. Khan,² and Babau R. Vishvakarma²

¹ Department of Electronics and Communication, University of Allahabad, Allahabad, India; Corresponding author: jaansari@rediffmail.com

² Department of Electronics Engineering, IT, BHU, Varanasi 221005, India

Received 21 April 2008

ABSTRACT: In this article, analysis of V-slot loaded patch antenna is proposed using equivalent circuit model. Such antenna provides a wide bandwidth which depends inversely on the base width and slot thickness. The proposed results are compared with experimental and simulated results which are in good agreements. Radiation pattern of the proposed antenna is in good agreement with the simulated results. This validates the accuracy of the proposed model. © 2008 Wiley Periodicals, Inc. *Microwave Opt Technol Lett* 50: 3069–3075, 2008; Published online in Wiley InterScience (www.interscience.wiley.com). DOI 10.1002/mop.23891

Key words: patch antenna; wide-band; microstrip antenna; V-slot loaded patch

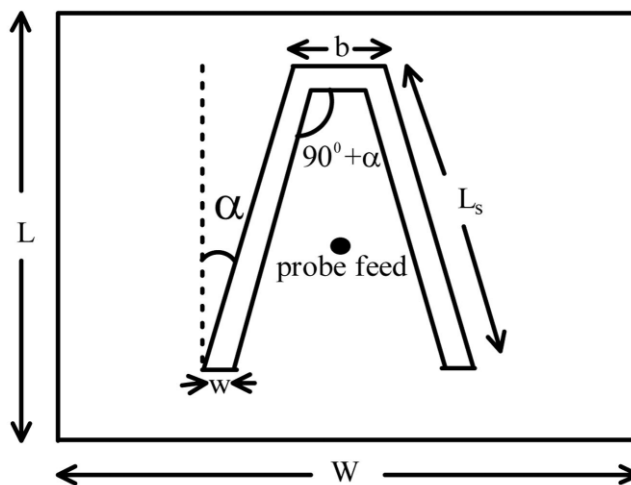
1. INTRODUCTION

Because of the limitation of the narrow operating bandwidth, numerous techniques have been proposed to enhance the bandwidth of microstrip patch antenna [1, 2] such as antenna loaded with U-slot [3], utilizing the shorting pin or shorting wall [4, 5], cutting the slot in the patch such as probe-fed U-slot patch [6] double-C shape patch antennas [7], and E-shaped patch antenna [8]. Further stacked patch configuration provides increased bandwidth characteristics [9]. In this article, a V-slot loaded rectangular microstrip patch antenna has been analyzed. V-slot loaded patch provides additional parameters than a U-slot loaded patch [6]. As this antenna has more coupled resonators, a wideband characteristic of the antenna is obtained.

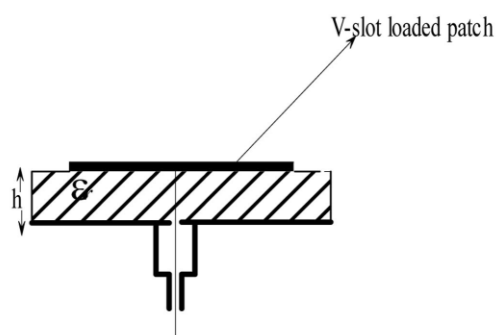
In the present analysis the antenna performance is evaluated for different values of V-slot arm length, base width, V-arm angle, and slot width. The entire investigations are compared with the simulated and experimental results [10].

2. THEORETICAL CONSIDERATIONS

Figure 1 shows V-slot loaded patch which is coaxially fed at the center of the patch. The theoretical analysis of the proposed antenna is derived by considering the two slots along the radiating edges as an inclined slot of the length “ L_s ” at an angle “ α ” and a base slot at an angle $(90^\circ + \alpha)$ which is along nonradiating edge of the patch.



(a) Top view



(b) side view

Figure 1 Geometry of V-slot loaded patch

An inclined slot in the patch is analyzed using the duality relationship between the dipole and slot [11]. Considering the coordinate of the slot (x_1, y_1) the longitudinal component of current into the inclined slot is given as [12]

$$I(y_1) = I_m \cos(\alpha) \sin \left[k \left(\frac{L_s}{2} - y_1 \right) \right] y_1 > 0$$

$$= I_m \cos(\alpha) \sin \left[k \left(\frac{L_s}{2} + y_1 \right) \right] y_1 < 0 \quad (1)$$

where I_m = maximum current in the inclined slot; L_s = length of the slot

$$k = \frac{2\pi}{\lambda}$$

and α = inclination angle.

The Poynting vector associated with the inclined slot can be written as

$$P_r = \frac{1}{2} |E_\theta| |H_\phi| = \frac{|E_\theta|^2}{2\eta_0} \quad (2)$$